FAST AND ACCURATE DESIGN TOOL FOR ROTATIONALLY SYMMETRIC REFLECTOR ANTENNAS WITH 3D WAVEGUIDE COMPONENTS AND SUPPORT STRUCTURES

E. Jørgensen[1], **P. Meincke**[1], **and M. Sabbadini**[2]

[1]*TICRA, Læderstræde 34, DK-1201 København K, Denmark, ej@ticra.com, pme@ticra.com*
[2]*ESA/ESTEC, 2200 AG Noordwijk, The Netherlands, Marco.Sabbadini@esa.int*

ABSTRACT

We present a new efficient design tool for rotationally symmetric reflector antennas, possibly including 3D support structures and waveguide components. The tool is based on a combination of four solvers: Mode-Matching (MM) for cylindrical wave-guiding structures, a newly developed higher-order BoR-MoM for rotationally symmetric structures, higher-order 3D MoM for arbitrary waveguide components or reflector support structures, and PO for extremely large reflectors. These four solvers are combined using a rigorous domain decomposition approach based on scattering and admittance matrices, and the concept of radiation ports is introduced to decouple multiple scatterers located in free space. The admittance matrices of the unchanged parts can then be reused during the optimization phase, thus significantly reducing the time to rebuild the full solution. An example reflector design shows significantly improved performance compared to previously published results.

Key words: Body of Revolution, Method of Moments, higher-order basis functions, mode-matching, domain decomposition, scattering matrix, maritime user terminals.

1. INTRODUCTION

Rotationally symmetric reflector systems are commonly applied for compact high-gain antennas with low manufacturing costs, low sidelobes, and low cross polarization. The typical application areas are maritime user terminals, radar systems, and point-to-point links. These compact systems often employ two reflectors in a classical axially displaced reflector configuration [1], or alternatively, a single reflector with a backward radiating hat feed [2, 3]. A common feature of these compact systems is a very tight integration of feed, subreflector, dielectric support structure, and main reflector, which leads to a resonant structure that cannot be analyzed with high-frequency methods. Instead, a full-wave model is needed to analyze the system with sufficient accuracy and consequently, the full-wave model is also needed when numerically optimizing the antenna performance. Commercially available software for general 3D problems lead to prohibitively long run-times and do not allow numerical optimization. Instead, the rotational symmetry of the structure has been used to formulate the Body-of-Revolution Method of Moments (BoR-MoM) [4] which is available in a few commercial tools. The BoR-MoM equations are typically discretized with triangular basis functions that require 15 unknowns per wavelength to achieve convergence. This leads to a typical run time of 30-60 seconds per frequency point for a compact antenna. This speed is not sufficient for a full optimization of the combined system including the surface shape of the reflectors. In addition, many terminal antennas based on rotationally symmetric reflectors include small 3D features, e.g., waveguide components with arbitrary cross section. The presence of 3D geometry prevents the use of BoR-MoM and leaves a prohibitively slow 3D analysis as the only option.

This paper presents an efficient design tool for rotationally symmetric reflector antennas, possibly including 3D parts. The analysis core of the tool is based on a combination of four efficient solvers:

- The recently developed higher-order BoR-MoM is used for rotationally symmetric reflectors, radomes, dielectric support structures, and lenses. The higher-order formulation is based on hierarchical basis functions and smooth curvilinear patches, which imply that even large structures can be handled with very few unknowns. The typical runtime for a full-wave analysis of a 40λ reflector system is 1-2 seconds on a laptop.
- The Mode-Matching (MM) algorithm [5] has been available for decades and provides excellent modeling speed and accuracy for cylindrical horns and wave-guiding structures. The implementation used in this work is a generalized version of the commercially available CHAMP software [6].
- The higher-order 3D MoM is used for waveguide components with arbitrary cross section and for reflector support structures. The implementation used here is derived from the GRASP software [7].
- Physical Optics (PO) is included for electrically huge reflectors.

The four solvers listed above are combined using a rigorous domain decomposition approach based on scattering and admittance matrices. This approach is routinely applied for analysis of wave-guiding structures where the scattering/admittance matrices of the individual components are cascaded to form the total scattering/admittance matrix. In this process, the internal waveguide ports are eliminated. In this work, we extend the admittance matrix formulation to the free space region containing multiple separate or connected scatterers, that are decoupled using so-called radiation ports. Previous works have employed spherical waves as port expansion function, e.g. [8, 9], but spherical radiation ports are not applicable to closely spaced or connected scatterers. In this work, BoR-MoM patches are used to represent the port geometry and BoR-MoM basis functions are used as port expansion functions, which allows rotationally symmetric radiation ports of general shape. The radiation port concept serves as a flexible framework for combining the multiple solvers and at the same time allows a scatterer, e.g. a reflector or a 3D support structure, to be characterized by an admittance matrix. The admittance matrices of the unchanged parts can be reused during the optimization phase, thus significantly reducing the time to rebuild the full solution.

The paper is structured as follows: The higher-order BoR-MoM and 3D MoM are outlined in Sections 2 and 3, respectively. The domain decomposition approach is described in Section 4 and the capabilities of the software tool are listed in Section 5. In Section 6, an example antenna design has been performed to illustrate that the high analysis speed can lead to significant performance improvements, even when compared to an already optimized antenna.

2. HIGHER-ORDER BOR-MOM FOR FAST FULL-WAVE ANALYSIS

The BoR-MoM has been formulated previously in several works, e.g., for conducting objects [4], for dielectric objects [10], and for composite metallic/dielectric objects [11]. All these works have employed triangular basis functions on flat curve segments which require a relatively large number of unknowns to achieve convergence. In this work, we employ the same continuos integral equation as in previous works, e.g., that of [11], but the equation is discretized with higher-order basis functions and curved segments of up to 4th order. The basis functions applied here are those of [12] which have been adapted to the present case with rotational symmetry. The electric and magnetic surface currents on each curve segment are expanded as

$$\begin{aligned}\mathbf{X} = &\sum_{m=0}^{M^\phi}\sum_{n=0}^{N^t} a_{mn}^{t,e}\mathbf{B}_{mn}^{t,e} + a_{mn}^{t,o}\mathbf{B}_{mn}^{t,o} \\ &+ \sum_{m=0}^{M^\phi}\sum_{n=0}^{N^t-1} a_{mn}^{\phi,e}\mathbf{B}_{mn}^{\phi,e} + a_{mn}^{\phi,o}\mathbf{B}_{mn}^{\phi,o}\,,\end{aligned} \tag{1}$$

where $\mathbf{X} = \mathbf{J}, \mathbf{M}$, $a_{mn}^{t,e}$, $a_{mn}^{t,o}$, $a_{mn}^{\phi,e}$, and $a_{mn}^{\phi,o}$ are unknown coefficients, N^t is the polynomial expansion order along the generatrix, M^ϕ is the azimuthal mode index, and $\mathbf{B}_{mn}^{t,e}$, $\mathbf{B}_{mn}^{t,o}$, $\mathbf{B}_{mn}^{\phi,e}$, and $\mathbf{B}_{mn}^{\phi,o}$ are $t-$ and ϕ-directed vector basis function defined as

$$\mathbf{B}_{mn}^{t,\binom{e}{o}}(t,\phi) = \frac{\mathbf{a}_t}{\mathcal{J}_s(t,\phi)}\widetilde{P}_n(t)\begin{pmatrix}\cos m\phi \\ \sin m\phi\end{pmatrix}, \tag{2a}$$

$$\mathbf{B}_{mn}^{\phi,\binom{e}{o}}(t,\phi) = \frac{\mathbf{a}_\phi}{\mathcal{J}_s(t,\phi)}P_n(t)\begin{pmatrix}\cos m\phi \\ \sin m\phi\end{pmatrix}, \tag{2b}$$

where $\mathbf{a}_t = \partial\mathbf{r}/\partial t$, $\mathbf{a}_\phi = \partial\mathbf{r}/\partial\phi$, and $\mathcal{J}_s(t,\phi) = |\mathbf{a}_t \times \mathbf{a}_\phi|$. In Eq. (2b), the polynomials $P_n(t)$ along the direction transverse to the current flow are chosen to be Legendre polynomials due to their nice properties [12]. In the direction along the current flow in Eq. (2b), the modified Legendre polynomials

$$\widetilde{P}_n(t) = \begin{cases} 1-t, & n=0 \\ 1+t, & n=1 \\ P_n(t) - P_{n-2}(t), & n \geq 2 \end{cases} \tag{3}$$

are used. The polynomials in (3) are zero at $t = \pm 1$ for $n > 1$ which implies that the high-order terms do not contribute to the current continuity. The two lowest order polynomials can be matched with the corresponding functions on the neighboring segments, or alternatively, they can be left out at external nodes. The modal expansion order, M^ϕ, should be adjusted to the specific problem and for a problem excited by the fundamental TE_{11} mode it is sufficient to include $m = 1$. The expansion order along the generatrix, N^t, is adapted to the electrical length of each segment which is usually in the order of 2λ. The BoR patches, obtained by rotation of a single curved segment, are illustrated in Figure 1 for the case of 1st, 2nd, and 3rd order segments. When higher-order basis functions and curved segments are used, the number of unknowns is reduced by a factor of 4 and drops to about 3-4 per wavelength, implying that the system matrix is easily stored and inverted, even for structures larger than several hundred wavelengths. The bottleneck for smaller problems is usually the matrix fill time which, however, can be dramatically reduced by using analytical techniques [13].

3. HIGHER-ORDER 3D MOM

The new design tool includes a higher-order 3D MoM solver, which is commercially available in the GRASP software package for reflector antenna modeling and scattering analysis [7]. In the new tool, the 3D MoM solver has been successfully applied to arbitrarily shaped waveguide components, where the higher-order formulation has proven both accurate and stable. Dielectric objects and composite metallic/dielectric objects are handled via the generalized PMCHWT [14] and the electric and magnetic surface currents on each patch are expanded as

$$\mathbf{X} = \sum_{m=0}^{M^u}\sum_{n=0}^{M^v-1} a_{mn}^{u}\mathbf{B}_{mn}^{u} + \sum_{m=0}^{M^v}\sum_{n=0}^{M^u-1} a_{mn}^{v}\mathbf{B}_{mn}^{v}\,, \tag{4}$$

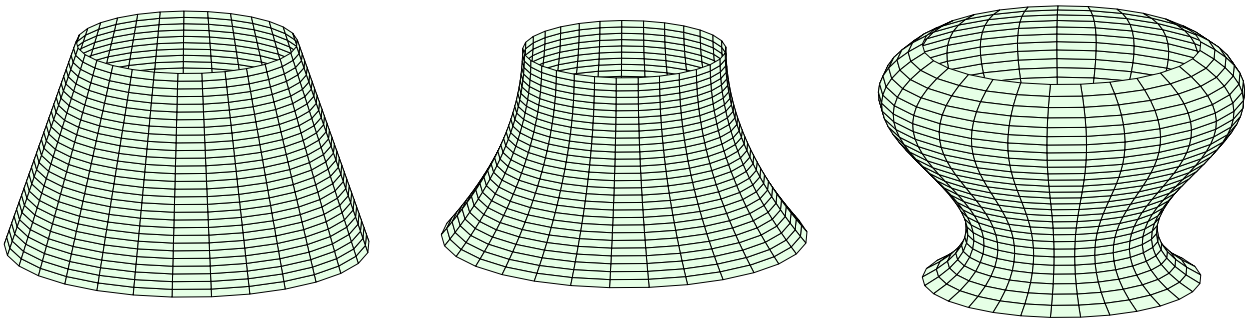

$$\mathbf{r}(t,\phi) = \sum_{i=0}^{p} l_i(p,t)\left(\hat{x}\rho_i\cos(\phi) + \hat{y}\rho_i\sin(\phi) + \hat{z}z_i\right), \quad -1 \le t \le 1, \quad -\pi \le \phi \le \pi, \quad l_i(p,t) = \prod_{\substack{k=0 \\ k\neq i}}^{p} \frac{t-t_k}{t_i-t_k}$$

Figure 1. Surfaces realized using a single BoR patch of first (left), second (centre), and third order (right), respectively. The generatrix is represented by a Lagrange polynomial passing through the interpolation nodes (ρ_i, z_i), where $1 \le i \le p+1$, and p is the order of the patch. The cubic patches using 4 interpolation nodes per patch generally provides the highest accuracy for curved surfaces and is preferred for reflectors.

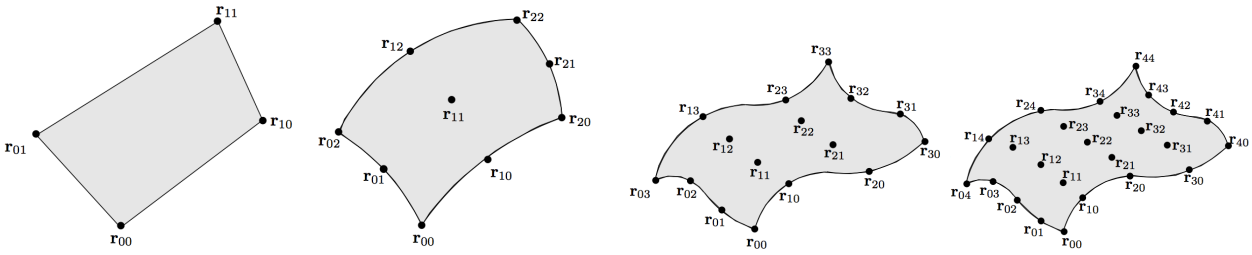

$$\mathbf{r}(u,v) = \sum_{i=0}^{p}\sum_{j=0}^{p} \mathbf{r}_{ij} l_i(p,u) l_j(p,v), \quad -1 \le u,v \le 1, \qquad l_i(p,u) = \prod_{\substack{k=0 \\ k\neq i}}^{p} \frac{u-u_k}{u_i-u_k}$$

Figure 2. Illustration of 3D surface patches, from left to right: Bilinear quadrilaterals defined by 4 interpolation nodes, biquadratic quadrilateral defined by 9 interpolation nodes, bicubic quadrilaterals defined by 16 interpolation nodes, and 4th-order quadrilaterals defined by 25 interpolation nodes. The parametric expression for the surface patches contains the interpolation nodes $\mathbf{r}_{ij}$ and $l_i(p,u)$ is the ith Lagrange polynomial of order p in which u_k is the parametric coordinate of the interpolation node.

where $\mathbf{X} = \mathbf{J}, \mathbf{M}$, a^u_{mn} and a^v_{mn} are unknown coefficients, M^u and M^v are the expansion orders along the u- and v-directions, and $\mathbf{B}^u_{mn}$ and $\mathbf{B}^v_{mn}$ are $u-$ and v-directed vector basis function defined as

$$\mathbf{B}^u_{mn}(u,v) = \frac{\mathbf{a}_u}{\mathcal{J}_s(u,v)} \widetilde{P}_m(u)\, P_n(v)\,, \tag{5a}$$

$$\mathbf{B}^v_{mn}(u,v) = \frac{\mathbf{a}_v}{\mathcal{J}_s(u,v)} \widetilde{P}_m(v)\, P_n(u)\,. \tag{5b}$$

Herein, $\mathbf{a}_u = \partial\mathbf{r}/\partial u$, $\mathbf{a}_v = \partial\mathbf{r}/\partial v$, $\mathcal{J}_s(u,v) = |\mathbf{a}_u \times \mathbf{a}_v|$ is the surface Jacobian, and the polynomials $\widetilde{P}_m$ are defined in Eq. (3). The polynomial orders M^u and M^v are adjusted to the electrical size of each patch, which is usually up to $2\lambda \times 2\lambda$. The curvilinear patches used here, as well as the parametric representation of the patches, are shown in Figure 2.

4. DOMAIN DECOMPOSITION ALGORITHM

Analysis and optimization of waveguide devices are routinely performed by computing scattering or admittance matrices of each component separately and using a cascading procedure to obtain the overall system response. This rigorous approach has the following advantages:

1. The computational cost of solving multiple small problems, and using cascading, is usually much lower than the cost required for solving one large problem.

2. Each component may be analyzed and optimized independently using the optimal analysis algorithm for the component in question.

3. When optimizing a system composed of multiple components, only the component being changed needs to be re-analyzed. The time to assemble the full solution is then a fraction of the time used for the initial analysis of the system.

For waveguide devices, the different components can be decoupled by introducing a number of waveguide ports with an associated set of port expansion functions. The

port expansion functions are usually chosen as the eigenvectors of a waveguide with the same cross section as the waveguide port. This choice leads to relative small scattering or admittance matrices as well as high accuracy.

The scattering/admittance matrix method described above may equally well be applied to a free-space region with a number of isolated or connected scatterers. The scatterers may then be separated by enclosing them in a port surface and defining suitable port expansion functions on that surface. The advantages listed in the previous paragraph are maintained by this approach. However, only a limited number of works have attempted such a solution, e.g., [8] for the case of coupling between a feed and a reflector, or [9] for an antenna placement problem. These works have employed spherical vector waves as port expansion functions, which leads to a relatively compact scattering or admittance matrix. However, the use of spherical vector waves imply that only spherical port surfaces may be used. This is a severe limitation for closely separated or connected scatterers.

In the present work, we use an admittance matrix description of a region of space, that may contain one or more scatterers and one or more waveguide apertures. The region is enclosed by a number of port surfaces and these ports are denoted radiation ports. The geometry of the radiation port may be represented as a surface mesh and standard MoM basis functions are used as port expansion functions. The radiation ports enclosing the region, and optionally the waveguide apertures or a conducting part of a scatterer, must define a single closed surface that act as a boundary of the region being characterized. Alternatively, the region may be defined by the space outside a closed surface and extending to infinity. The admittance matrix of such a region is obtained by MoM as described in Section 4.1 below. Furthermore, Section 4.2 lists the port types and port expansion functions implemented in the new software tool.

4.1. Extraction of Admittance Matrices

The admittance matrix of an arbitrarily shaped closed waveguide region with N waveguide ports can be obtained by MoM, e.g., by following the procedure detailed in [15]. In the present work, we use the same approach for extracting the admittance matrix of a region enclosed by multiple waveguide and radiation ports. The region may contain one or more composite metallic/dielectric scatterers. Consider the geometry shown in Figure 3.(a) that shows a waveguide aperture illuminating two scatterers (A and B). We wish to obtain an admittance matrix of the region containing the waveguide aperture and scatterer A. To this end, we introduce the radiation port shown with a red line in Figure 3.(b) and the waveguide port shown with a blue line. The region is now bounded by a closed surface consisting of the red and the blue surfaces, as well as a part of the exterior waveguide wall, which is considered to be a part of the scatterer. The space outside the region containing scatterer A is denoted region I and the space inside is denoted region II. In the following we assume that an impressed field, e.g., an incoming guided wave, may exist in region I. By using the surface equivalence principle, we close the port boundaries, denoted $S^p = S^{rp} + S^{wp}$, by a PEC surface and define equivalent magnetic port currents on this surface as

$$\mathbf{M}^p(\mathbf{r}) = -\hat{n} \times \mathbf{E}(\mathbf{r}) \tag{6}$$

where $\hat{n}$ is a unit normal directed from region I into region II. These magnetic port currents maintain the total electric field at the port surface. The continuity of the magnetic field at the port interface requires

$$\mathbf{H}^I_{\text{tan}}(-\mathbf{M}^p) + \mathbf{H}^i_{\text{tan}} = \mathbf{H}^{II}_{\text{tan}}(\mathbf{M}^p)\,, \tag{7}$$

where $\mathbf{H}^I(-\mathbf{M}^p), \mathbf{H}^{II}(\mathbf{M}^p)$ denote the magnetic field radiated in regions I and II, respectively, and $\mathbf{H}^i$ is the impressed magnetic field in region I. The magnetic port current is now expanded as

$$\mathbf{M}^p(\mathbf{r}) = \eta_0 \sum_{i=1}^{N^p} V_i \mathbf{M}^p_i, \tag{8}$$

where η_0 is the free space impedance and N^p is the number of port expansion function. By choosing N^p port weighting functions $\mathbf{W}^p_j$ and forming inner product with (7), we obtain the matrix equation

$$[I^p] = \left[Y^I + Y^{II}\right][V] \tag{9}$$

in which $[I^p]$ is related to the impressed field as

$$[I^p] = \left[\left\langle \mathbf{W}^p_j; \mathbf{H}^i_{\text{tan}} \right\rangle\right], \quad j = 1, ..., N^p \tag{10}$$

and $\left[Y^{I,II}\right]$ are the normalised admittance matrices

$$\left[Y^{I,II}\right] = \eta_0 \left[\left\langle \mathbf{W}^p_j; \mathbf{H}^{I,II}_{\text{tan}}(\mathbf{M}^p_i) \right\rangle\right]. \tag{11}$$

We now use the electric field integral equation (EFIE) to obtain the admittance matrix $\left[Y^{II}\right]$ that fully characterizes region II. The total electric field in region I is

$$\begin{aligned}\mathbf{E}(\mathbf{r}) = &-\nabla \times \int_{S^p} \mathbf{M}^p(\mathbf{r}')G\, dS' \\ &- \frac{j\eta_0}{k_0}\nabla \times \nabla \times \int_{S^p + S^{sc}} \mathbf{J}(\mathbf{r}')G\, dS'\end{aligned} \tag{12}$$

where S^p is the port surface, S^{sc} is the surface of the scatterers located inside region II, and $G = \exp(-jkR)/(4\pi R)$, $R = |\mathbf{r} - \mathbf{r}'|$. In (12) it has been assumed that the scattering object is PEC. If the scatterer contains dielectric materials, an additional magnetic current appears in (12) and the PMCHWT equations are used instead. The general form, which allows dielectrics, has been implemented in the tool but the additional terms are left out for simplicity. By restricting the observation point to the surface $S^p + S^{sc}$, and using Equation (6), we may

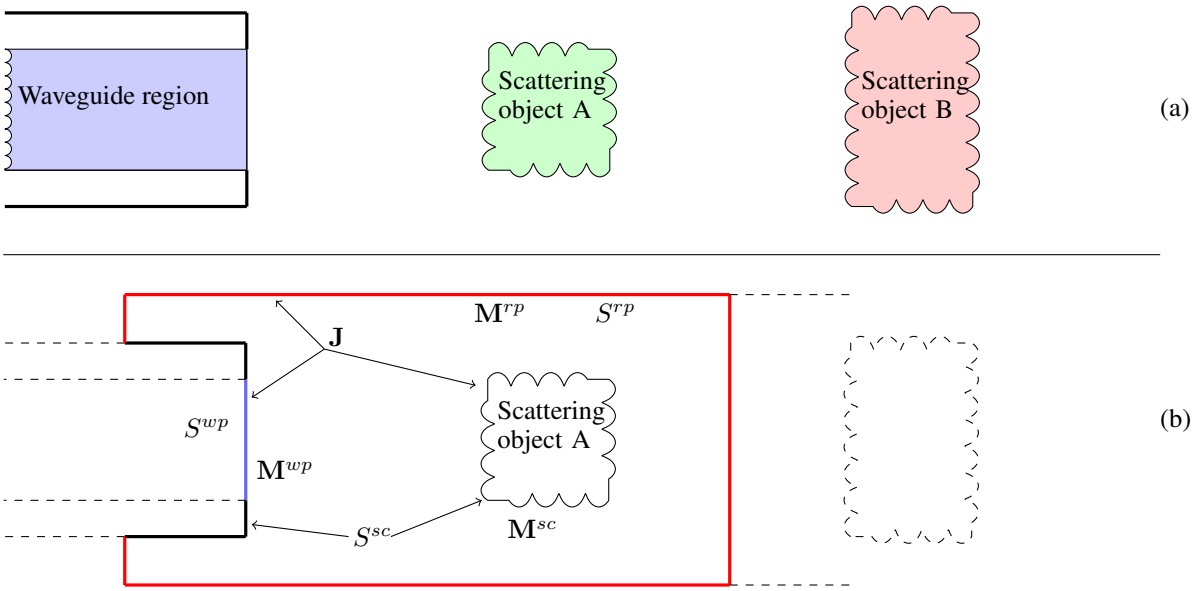

Figure 3. Top: A waveguide aperture is illuminating two scattering objects. Bottom: Equivalent problem for extraction of the admittance matrix of the region containing scattering object A. The waveguide aperture is closed by a waveguide port defined on the blue surface S^{wp}. The surface of scattering object A and the outer waveguide wall is denoted S^{sc}. The region is bounded by a radiation port located in free space. The surface of this radiation port is denoted S^{rp} and is shown in red. The waveguide port and the radiation port is closed by a PEC surface. Electric MoM basis functions $\mathbf{J}$ are defined on the surface $S_{sc} + S_{wp} + S_{rp}$, magnetic waveguide port basis functions $\mathbf{M}^{wp}$ are defined on S^{wp}, magnetic radiation port basis functions $\mathbf{M}^{rp}$ are defined on S^{rp}, and magnetic MoM basis functions $\mathbf{M}^{sc}$ are defined on the dielectric parts of the scattering object.

now write the EFIE as

$$\left[-\frac{j\eta_0}{k_0}\nabla\times\nabla\times\int\limits_{S^p+S^{sc}}\mathbf{J}(\mathbf{r}')G\,dS'\right]_{\tan} = \hat{n}\times\mathbf{M}^p(\mathbf{r}) + \left[\nabla\times\int\limits_{S^p}\mathbf{M}^p(\mathbf{r}')G\,dS'\right]_{\tan}. \quad (13)$$

The electric current $\mathbf{J}$ on $S^p + S^{sc}$ is now expanded as

$$\mathbf{J}(\mathbf{r}) = \sum_{t=1}^{N} I_t\mathbf{J}_t. \quad (14)$$

The electric current (14) and the magnetic port current (8) are now inserted in (13), and weighting functions $\mathbf{T}_s$, $s = 1, ..., N$, are chosen. By taking inner products of $\mathbf{T}_s$ and (13) we obtain the matrix equation

$$[Z]\,[I] = [P]\,[V] \quad (15)$$

where $[Z]$ is the standard EFIE impedance matrix

$$[Z] = \frac{-j}{k_0}\left\langle \mathbf{T}_s; \nabla\times\nabla\times\int\limits_{S^p+S^{sc}}\mathbf{J}_t G\,dS'\right\rangle \quad (16)$$

and $[P]$ is the $N \times N^p$ matrix defined as

$$[P] = \left\langle \mathbf{T}_s; \hat{n}\times\mathbf{M}_i^p + \nabla\times\int\limits_{S^p}\mathbf{M}_i^p G\,dS'\right\rangle \quad (17)$$

Equation (15) allows the coefficients I_t in (14) to be determined as

$$[I] = [Z]^{-1}\,[P]\,[V]\,. \quad (18)$$

At the port surface S^p, the magnetic field must satisfy $\mathbf{J} = \hat{n}\times\mathbf{H}^{II}_{\tan}(\mathbf{M}^p)$, which also may be written as

$$-\hat{n}\times\mathbf{J} = \mathbf{H}^{II}_{\tan}(\mathbf{M}^p). \quad (19)$$

We now insert (14) and (8) in (19) and perform inner products with the port weighting functions $\mathbf{W}_j^p$, which leads to the matrix equation

$$[Q]\,[I] = \left[Y^{II}\right]\,[V] \quad (20)$$

where $\left[Y^{II}\right]$ is the desired admittance matrix defined in (11) and $[Q]$ is a $N^p \times N$ matrix given by

$$[Q] = \left\langle \mathbf{W}_j^p; -\hat{n}\times\mathbf{J}_t\right\rangle. \quad (21)$$

By comparing (18) and (20), we have finally found the admittance matrix of region II as

$$\left[Y^{II}\right] = [Q]\,[Z]^{-1}\,[P]\,. \quad (22)$$

4.2. Port Expansion Functions and Geometric Representation

The rigorous domain decomposition approach employs two port types: Waveguide ports and radiation ports. For

Table 1. List of port types and port geometry, associated port expansion functions, and supported analysis methods.

Port type	Port Geometry	Port Expansion Functions	Supported Analysis Algorithm			
			Mode Matching	BoR-MoM (Section 2)	3D MoM (Section 3)	PO
Circular/coaxial waveguide port	Circular disc / planar ring	Circular/coaxial waveguide eigenvectors	x	x	x	
Rectangular waveguide port	Planar rectangle	Rectangular waveguide eigenvectors			x	
Radiation port	Rotationally symmetric surface defined as a BoR mesh (Figure 1)	BoR-MoM basis functions (Equation (2))		x	x	x

waveguide ports, the port expansion functions are chosen as $\hat{n} \times \mathbf{e}_{mn}$ where $\hat{n}$ is a unit normal vector to the port and $\mathbf{e}_{mn}$ are the orthonormal electric eigenvectors of the waveguide. For radiation ports, we have chosen to use the BoR patches in Figure 1 and the basis functions in Eq. (2) to represent the port geometry and the port expansion functions, respectively. This choice results in a very low number of port expansion functions and consequently a compact admittance matrix. In addition, the admittance matrix of a circular symmetric region is a block-diagonal matrix where each block corresponds to a single azimuthal m-index that may be computed and stored separately. An overview of the port types and port expansion functions currently used in the software tool is shown in Table 1.

5. DESIGN TOOL BASED ON FOUR RIGOROUSLY COUPLED SOLVERS

The four efficient solvers and the rigorous domain decomposition algorithm described above have been integrated in a flexible design software that combines all the required capabilities in a single tool. The tool provides a fast full-wave analysis of rotationally symmetric reflectors systems, even when the geometry contains minor 3D parts. As an example of the analysis speed, the computation times for various ring-focus antennas are listed in Figure 4. It can be observed that a full-wave analysis of a 50λ rotationally symmetric ring-focus antenna is accomplished in slightly more than one second when running on a laptop computer. These results have been obtained using the BoR-MoM solver and a circular waveguide port for extraction of the scattering parameters.

In addition to the core analysis methods, the software contains a rich set of parametric models for definition of the geometry. The geometry can be defined in several ways with increasing level of details, ranging from a high-level model with few parameters to a fine-grained model with a large number of optimization variables. Reflector surfaces and horn profiles are conveniently defined as splines with user-specified and optimizable control points. The tool includes four optimization algorithms, both global optimization and gradient-based algorithms, as well as several built-in optimization goals,

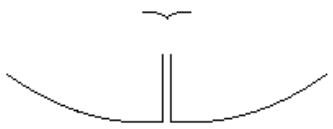

Main reflector diameter	Computation time
15λ	0.2 s
25λ	0.3 s
40λ	0.7 s
50λ	1.2 s
75λ	3.0 s
100λ	5.7 s

Figure 4. Higher-order BoR-MoM computation times for a simple ring-focus dual-reflector reflector antenna, (laptop computer, 2011 model). The antenna geometry comprises a main reflector, a sub reflector, and the exterior wall of the feed horn. The feed horn is a simple open-ended waveguide and the reported computation time includes extraction of waveguide scattering parameters. The computation time per frequency are listed for antennas of different sizes.

e.g., return loss, directivity, side-lobe level, cross-polar radiation, and radiation pattern templates. The latter optimization goal is a convenient facility for meeting regulatory requirements on the radiation pattern.

6. EXAMPLE DESIGN OF A COMPACT ANTENNA WITH LOW SIDE-LOBES

The design tool is now tested with a practical antenna synthesis problem that has been published previously [16]. The antenna is a very small hat-feed reflector antenna with a main reflector diameter of 24 inches at 5.8 GHz, corresponding to 11.8λ. The requirements for this antenna are listed in Table 2. The feeding waveguide needs to be above cut-off and the small main reflector and the low sidelobe requirement limits the allowable size of the feed hat. These constraints make it a very challenging task to obtain a reasonable return loss and the solution of [16] therefore employed a small dielectrically filled

waveguide. In addition, the solid dielectric was extended to completely fill the space between the feed and the feed hat. This implies that a relatively large piece of dielectric material is needed, resulting in dielectric losses and a relatively high mass. With this configuration the pattern requirements were met but the return loss was 12 dB [16] when the main reflector was included.

The new design tool has been used to design an alternative antenna of the same size but without dielectric filling in the waveguide. Instead, the feed hat is supported by a thin dielectric cone with a relative permittivity of 2.5. The feed hat is designed with a stepped profile and the main reflector is highly shaped to force the sidelobes down. The antenna was optimized using a total of 32 optimization variables and the geometry of the optimized design and the radiation pattern are shown in Figure 5. Table 3 lists the performance parameters of the designed example as well as the original design proposed in [16]. The example design presented here differs significantly from that of [16] by providing a higher directivity, lower sidelobes, a much higher return loss, and lower cross-polar radiation, while avoiding the need for a dielectrically filled waveguide. The major improvements observed in Table 3 have been accomplished by allowing a highly shaped main reflector and a stepped sub reflector, which results in a high number of optimization variables. Nevertheless, the fast analysis provided by the new tool made this design task a relatively easy job. This design was performed without using radiation ports, i.e., primarily using the BoR-MoM solver.

Table 2. Design Requirements for a compact reflector system, from [16]

Frequency Range	5.725 - 5.875 GHz
Aperture diameter	24 in (0.61 m $\approx 11.8\lambda$)
Maximum VSWR	1.5:1 (ret. loss 14 dB)
Polarization	V or H
Antenna gain	27.5 dBi
Sidelobe level relative to peak	-20 dB
Maximum cross-polarization level relative to co-polar peak	-25 dB

7. CONCLUSIONS

We have presented the development of new design tool for rotationally symmetric reflector systems, possibly including 3D waveguide components and support structures. The tool is based on four efficient solvers: Mode Matching for circular horns, higher-order BoR-MoM for reflectors and dielectric support structures, higher-order 3D MoM for 3D waveguide components and support structures, and PO for electrically huge reflectors. The four solvers are combined using a rigorous domain decomposition approach based on scattering and admittance matrices. The admittance matrix method is extended to the region outside the horn by introducing radiation ports

Table 3. Realized performance parameters of compact reflector systems

	Design from [16]	This paper
Directivity	28.4 dBi	29.4 dBi
Return loss	$>$ 12 dB	$>$20 dB
Sidelobe level relative to peak	-25.9 dB	-26.0 dB
Maximum cross-polarization level relative to co-polar peak	-20.5 dB	-28.0 dB

that decouple various regions of space. This allows a support structure or a reflector to be characterized by an admittance matrix that can be reused during the optimization phase, which potentially leads to a dramatic reduction of the time needed to repeatedly obtain the full-wave solution. However, this capability has not yet been backed by numerical results.

Numerical results obtained with the BoR-MoM solver have demonstrated that a full-wave analysis of a 50λ ring-focus antenna can be accomplished in slightly more than one second on a laptop computer. The design tool was finally tested on a previously published antenna synthesis problem. The compact antenna design shown here provides higher directivity (+1dB), higher return loss (+8dB), and lower cross-polar radiation (-7.5 dB), while avoiding the need for a dielectrically filled waveguide. This example illustrates that a fast and flexible design tool eventually leads to better antenna performance.

ACKNOWLEDGEMENTS

This work is supported by ESA/ESTEC within the ARTES 5.2 programme, ESTEC contract 4000104664/11/NL/US, and by the Danish National Advanced Technology Foundation, j.nr. 004-2010-1.

REFERENCES

1. Moreira, F.J.S. & Prata, A. (2001). Generalized classical axially symmetric dual-reflector antennas, *IEEE Trans. Antennas Propagat.*, **49(4)**, pp. 547–554.

2. Kildal, P.S. (1987). The hat feed: a dual-mode rear-radiating waveguide antenna having low cross polarization, *IEEE Trans. Antennas Propagat.*, **AP-35(9)**, pp. 1010–1016.

3. Yang, J. & Kildal, P.S. (1998). FDTD design of a chinese hat feed for shallow mm-wave reflector antennas, in *1998 IEEE Antennas Propagat. Soc. Int. Symp.*, volume 4, 2046–2049.

4. Mautz, J.R. & Harrington, R.F. (1977). H-field, E-field, and combined field solutions for bodies of revolution, Technical Report TR-77-2, Syracuse University, NY, USA.

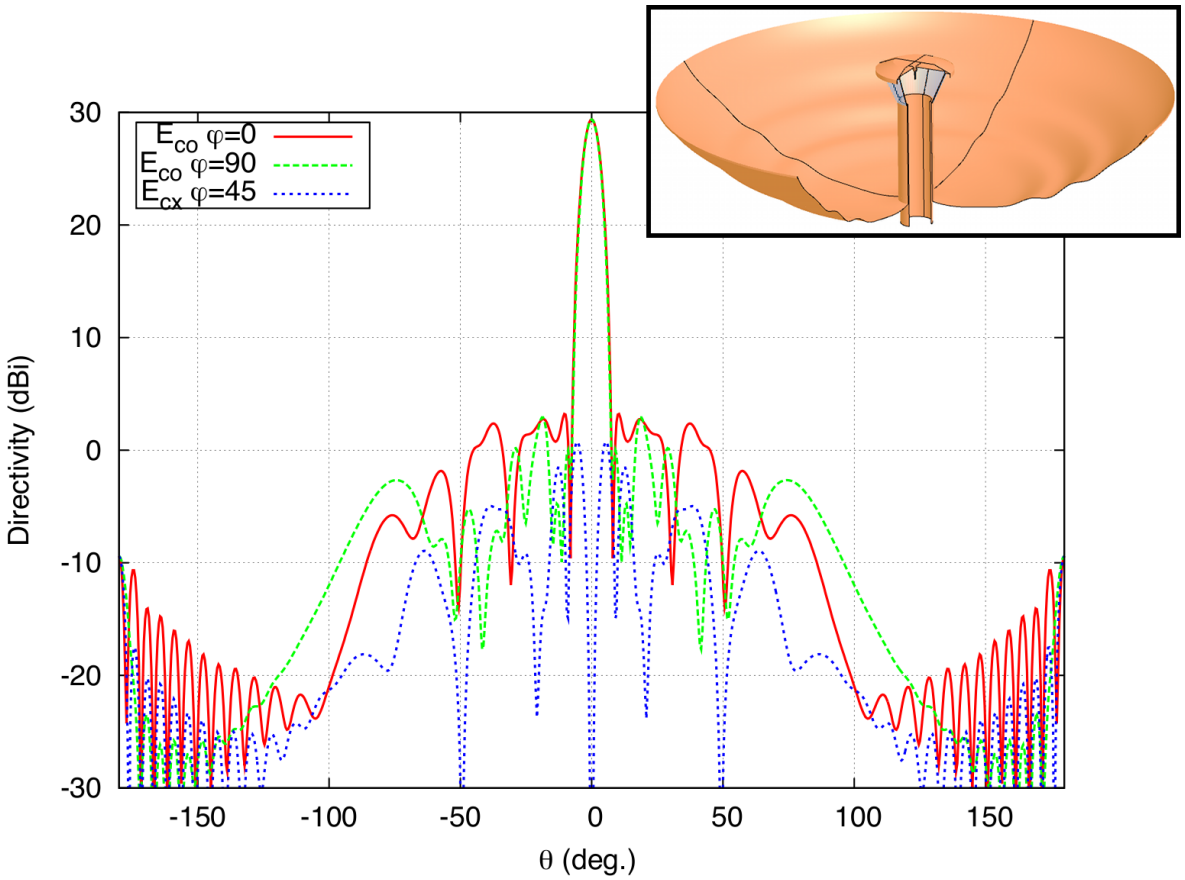

Figure 5. Radiation pattern of the 11.8λ *compact rotationally symmetric reflector antenna. Insert: The optimized geometry with a 45 degree cut-out. The dielectric support cone is shown in blue.*

5. Kühn, E. & Hombach, V. (1983). Computer-aided analysis of corrugated horns with axial or ring-loaded radial slots, in *3rd Internat. Conf. on Antennas and Propagation (ICAP 83)*, 127–131.

6. CHAMP v. 3.0, TICRA, Læderstræde 34, Copenhagen, Denmark, www.ticra.com.

7. General Reflector Analysis Program, G., TICRA, Læderstræde 34, Copenhagen, Denmark, www.ticra.com.

8. Giovampaola, C.D., Martini, E., Toccafondi, A. & Maci, S. (2010). Antenna mismatch induced by nearby scatterers through a spherical wave - generalized scattering matrix approach, *Electromagnetic Theory (EMTS), 2010 URSI International Symposium on*, pp. 776 – 779.

9. Barka, A. & Caudrillier, P. (2007). Domain decomposition method based on generalized scattering matrix for installed performance of antennas on aircraft, *Antennas and Propagation, IEEE Transactions on*, **55(6)**, pp. 1833 – 1842.

10. Wu, T.K. & Tsai, L.L. (1977). Scattering from arbitrarily-shaped lossy dielectric bodies of revolution, *Radio Science*, **12**, pp. 709–718.

11. Kishk, A.A. & Shafai, L. (1986). Different formulations for numerical solution of single or multibodies of revolution with mixed boundary conditions, *IEEE Trans. Antennas Propagat.*, **34(5)**, pp. 666–673.

12. Jørgensen, E., Volakis, J.L., Meincke, P. & Breinbjerg, O. (2004). Higher order hierarchical Legendre basis functions for electromagnetic modeling, *IEEE Transactions on Antennas and Propagation*, **52(11)**, pp. 2985–2995.

13. Gustafsson, M. (2010). Accurate and efficient evaluation of modal green's functions, *Journal of Electromagnetic Waves and Applications*, **24(10)**, pp. 1291–1301.

14. Kolundžija, B.M. (1999). Electromagnetic modeling of composite metallic and dielectric structures, *IEEE Trans. Microwave Theory and Techniques*, **47(7)**, pp. 1021–1032.

15. Bunger, R. & Arndt, F. (2000). Moment-method analysis of arbitrary 3-d metallic n-port waveguide structures, *IEEE Trans. Microwave Theory and Techniques*, **48(4)**, pp. 531 – 537.

16. Kishk, A.A. & Shafai, L. (2003). Small reflector antenna with low sidelobes, *IEEE Trans. Antennas Propagat.*, **51(10)**, pp. 2907–2912.